ACS APPLIED MATERIALS & INTERFACES

Research Article

www.acsami.org

In Situ Growth of Matchlike ZnO/Au Plasmonic Heterostructure for Enhanced Photoelectrochemical Water Splitting

Mi Wu, Wei-Jian Chen, Yu-Hua Shen, Fang-Zhi Huang, Chuan-Hao Li,* and Shi-Kuo Li*

Innovation Lab for Clean Energy and Green Catalysis, School of Chemistry and Chemical Engineering, Anhui University, Hefei 230601, P. R. China

Supporting Information

ABSTRACT: In this paper, we report a novel matchlike zinc oxide (ZnO)/gold (Au) heterostructure with plasmonic-enhanced photoelectrochemical (PEC) activity for solar hydrogen production. The matchlike heterostructure with Au nanoparticles coated on the tip of ZnO nanorods is in situ grown on a zinc (Zn) substrate by using a facile hydrothermal and photoreduction combined approach. This unique heterostructure exhibits plasmonic-enhanced light absorption, efficient charge separation and transportation properties with tunable Au contents. The photocurrent density of the matchlike ZnO/Au heterostructure reaches 9.11 mA/cm^2 at an applied potential of 1.0 V (vs Ag/AgCl) with an Au/Zn atomic ratio of 0.039, which is much higher than that of the pristine ZnO nanorod array (0.33 mA/cm^2). Moreover, the solar-to-hydrogen conversion efficiency of this special heterostructure can reach 0.48%, 16 times higher than that of the pristine ZnO nanorod array (0.03%). What is more, the efficiency could be further improved by optimizing the Au content of the heterostructure. The formation mechanism of such a unique heterostructure is proposed to explain the plasmonic-enhanced PEC performance. This study might contribute to the rational design of the visible-light-responsive plasmonic semiconductor/metal heterostructure photoanode to harvest the solar spectrum.

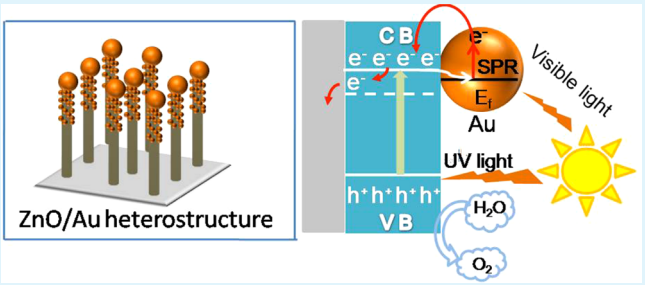

KEYWORDS: *photoreduction, matchlike ZnO/Au heterostructure, surface plasmon resonance, photoanode, PEC water splitting*

1. INTRODUCTION

Photoelectrochemical (PEC) water splitting using semiconductor photoelectrodes for hydrogen generation has been extensively explored because of its importance in the development of clean and renewable energy.[1−3] Among various semiconductor photoanode materials, metal oxides such as titanium dioxide (TiO_2), zinc oxide (ZnO), tungsten trioxide (WO_3), and hematite (α-Fe_2O_3) have been widely studied for their high photoelectric performance.[3−9] As a common and inexpensive semiconductor, ZnO materials with various nanostructures have emerged as promising photoanodes[7,10−13] because of their excellent electron mobility and electron-transfer efficiency (115−155 cm^2·V^{-1}·s^{-1}),[14] intrinsic stability, and favorable environmental compatibility. It has been reported that such a semiconductor photoanode can achieve a theoretical maximum photocurrent of 0.6 mA·cm^{-2}.[15] Vertically oriented ZnO nanorod/wire arrays provide optimal architectures as photoanodes because of their large surface area, long light-irradiation pathway, low recombination losses, and short diffusion length.[16,17] Nevertheless, their large band gap limits light absorption in the visible region of interest, which imposes a fundamental restriction on the overall photo-to-hydrogen efficiency.

Recently, the localized surface plasmon resonance (SPR) effect enhanced photoelectric conversion via a strong light scattering, and local field enhancement has received much attention.[18−24] SPR is a collective oscillation of the free conduction-band electrons at the interface between noble metal nanoparticles and dielectrics driven by the electromagnetic field of incident light in the visible and IR regions.[25] For gold (Au) nanoparticles, they can also absorb UV light because of their electron interband transitions from 5d to 6sp.[26] Also, importantly, Au nanoparticles are stable enough for preventing corrosion during the photoreaction. Many efforts have been attempted to design Au-nanoparticle-based plasmonic nanostructures for solar water splitting. Typically, Lee et al.[27] reported Au-decorated silicon/hematite core/shell nanowire arrays for sunlight-driven solar water splitting with an achieved efficiency of 6.0%. Lu et al.[20] demonstrated Au-modified TiO_2 electrodes with enhanced photoactivity by manipulating the shape of the Au nanostructures. Wang et al.[28] reported plasmonic Au nanocrystals coupled to TiO_2 nanotubes for visible-light-driven PEC water splitting, achieving a photoconversion efficiency of 1.1%. However, these synthesis procedures usually involve a complicated and time-consuming seed-mediated process and various harsh reaction conditions. Therefore, it is highly desirable to develop a simple and cost-

Received: May 17, 2014
Accepted: August 13, 2014
Published: August 21, 2014

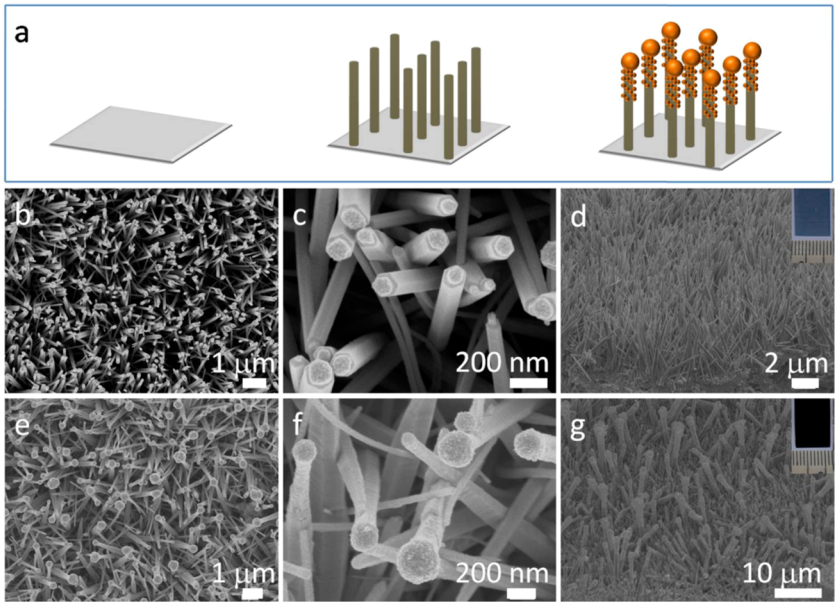

Figure 1. (a) Schematic illustration of the synthesis of a matchlike ZnO/Au heterostructure. (b and c) Top views. (d) Cross-sectional-view SEM images of ZnO nanorod arrays. (e and f) Top views. (g) Cross-sectional-view SEM images of the typical matchlike ZnO/Au heterostructure. The insets of parts d and g show substrate photographs of pristine ZnO nanorod arrays and the typical ZnO/Au heterostructure, respectively.

effective strategy for the scalable synthesis of a plasmonic heterostructure with light harvesting.

Herein, we report a novel matchlike ZnO/Au plasmonic heterostructure for PEC solar hydrogen production. This novel heterostructure is synthesized via a facile hydrothermal and photodeposition reduction process. First, the well-aligned ZnO nanorod array is directly grown on a zinc (Zn) foil through a hydrothermal approach without involving any seed-mediated process. Then a photoreduction method was used to deposit Au nanoparticles on the tip of ZnO nanorods, resulting in the formation of a matchlike ZnO/Au heterostructure. The amount of decorated Au nanoparticles can be rationally tailored by varying the reaction time. To the best of our knowledge, this is the first time to report a matchlike ZnO/Au heterostructure for plasmonic PEC water splitting. Importantly, such a novel heterostructure compared with other related studies presents some prominent merits: (1) in situ growth of the ZnO/Au heterostructure is simpler and more controllable; (2) the photoreduction process is green without using any surfactants; (3) the plasmonic effects of the tipped Au nanoparticles greatly promote light harvesting and accelerate charge transportation, which are important for enhancing the solar-to-hydrogen conversion efficiency. Therefore, the present work might be important for providing a facile protocol to prepare semiconductor/metal heterostructures with a plasmonic-enhanced PEC performance under the entire solar spectrum.

2. EXPERIMENTAL SECTION

2.1. Large-Scale in Situ Growth of ZnO Nanorod Arrays. The well-aligned ZnO nanorod arrays on a Zn foil were synthesized according to a modified hydrothermal method.[29] In a typical procedure, the commercial Zn foil (99.9%, 1 × 3 cm) was polished and washed with ethanol and deionized water sequentially under ultrasonication for 10 min. Then, a 1,6-hexanediamine aqueous solution consisting of 4 mL of 1,6-hexanediamine melted at 50 °C, and 36 mL of deionized water was transferred into a 50 mL Teflon-lined stainless steel autoclave, followed by immersion of the treated Zn foil into the solution. The autoclave was sealed and heated in an oven at 180 °C for 5 h, which was then allowed to cool to room temperature naturally. The Zn foil covered with a light-blue precipitate on both sides was thoroughly rinsed with distilled water and ethanol and then dried in a vacuum at 60 °C for 12 h.

2.2. Photoreduction Synthesis of Matchlike ZnO/Au Heterostructures with Tunable Au Contents. The matchlike ZnO/Au heterostructure with tunable Au contents was obtained via a photodeposition reduction process. Briefly, 1.5 mL of $HAuCl_4$ (3 mM) was first diluted into 50 mL of an aqueous solution with distilled water, which was then transferred into an 80 mL quartz glass tube. Subsequently, the as-prepared Zn foil covered with ZnO nanorod arrays was inserted into the solution with one side against the light source, which was then illuminated by a 300 W xenon lamp for 4 h to reduce Au^{3+} to Au^0. Finally, a uniform black film formed against the light side was washed with distilled water and ethanol several times and then kept in a vacuum at room temperature. The content of the decorated Au nanoparticles can be tailored by optimizing the irradiation time.

2.3. Characterization. Scanning electron microscopy (SEM) images were acquired with a Zeiss Supra 40 scanning electron microscope at an acceleration voltage of 5 kV. The transmission electron microscopy (TEM), energy-dispersive spectrometry (EDS), selected-area electron diffraction (SAED) pattern, and high-resolution transmission electron microscopy (HRTEM) images and scanning transmission electron microscopy energy-dispersive spectrometry (STEM-EDS) element mapping were obtained using a JEOL-2010F TEM instrument with an acceleration voltage of 200 kV. Prior to the measurements, the ZnO nanorod arrays and the matchlike ZnO/Au heterostructures were detached from the Zn substrate, ultrasonically dispersed in ethanol, dipped onto a copper grid with a lacey carbon film, and dried under ambient conditions. A powder X-ray diffraction (XRD) pattern was obtained using a Philips X'Pert PRO SUPER X-ray diffractometer equipped with graphite-monochromated Cu Kα radiation (λ = 1.54056 Å). X-ray photoelectron spectroscopy (XPS) measurement was performed on an X-ray photoelectron spectrometer (ESCALab MKII). Inductively coupled plasma results were obtained using an Optima 7300 DV instrument. Room temperature photoluminescence (PL) spectra were recorded using a fluorescence spectrophotometer (Hitachi F-4500) with an excitation wavelength of 390 nm. The UV−vis spectra were recorded with a spectrophotometer (Hitachi U-3900).

2.4. PEC Measurements. To perform the PEC tests, one end of the substrate was completely scratched to expose the Zn surface for

connecting the electrode clamp. A three-electrode PEC cell using a 100 mL 0.1 M Na_2SO_4 aqueous solution (pH = 7.0) as the electrolyte was carried out for the current density measurements. Also, before use, the electrolyte solution had been bubbled with a dinitrogen flow for 1 h to exclude the dissolved oxygen. The pristine ZnO nanorod array and matchlike ZnO/Au heterostructure substrates were used as the working electrodes, Ag/AgCl (1 M KCl) as the reference electrode, and a platinum foil as the counter electrode. Illumination was provided by a solar simulator using a 150 W xenon lamp and equipped with a 1.5 AM filter. The light power intensity at the sample positions was about 100 mW·cm^{-2}. An electrochemical workstation (CHI660D) was used to record the current density. A scan rate of 5 mV·s^{-1} was performed for linear sweep voltammetry (LSV; $J-V$ curves). The amperometric $I-t$ photoresponse was investigated under a bias voltage of 0.5 V (vs Ag/AgCl) with a light on−off interval of 100 s. Impedance measurements were carried out in the dark with the alternating-current (ac) voltage at 10 mV.

3. RESULTS AND DISCUSSION

The schematic illustration for the synthesis of a matchlike ZnO/Au heterostructure photoanode on a Zn foil is shown in Figure 1a. After immersion of a Zn foil into a 1,6-hexanediamine aqueous solution at an elevated temperature, a well-aligned ZnO nanorod array is in situ grown on the Zn foil surface. Then the as-prepared ZnO array is introduced into a $HAuCl_4$ aqueous solution, followed by irradiation of the xenon lamp to generate a ZnO/Au heterostructure. Typical SEM images of ZnO nanorod arrays are presented in Figure 1b−d. As can be seen, ZnO nanorods are vertically grown on the Zn foil surface with a high cover density. Also, the well-aligned nanorods present a smooth surface and tip. Importantly, these homogeneous nanorod arrays can be obtained over a large area on a Zn substrate (1 × 3 cm), as shown in the inset in Figure 1d. The length of the nanorods is about 4 μm with an average diameter in the range of 300−400 nm. Parts e−g of Figure 1 shows the typical SEM images of the ZnO/Au heterostructure. It can be clearly seen that spherical Au beads with a size of ca. 200 nm are located on the tips of the ZnO nanorods. It is worth noting that the spherical beads are composed of numerous small-sized Au nanoparticles. Interestingly, the obtained heterostructure seems like a match. The above results reveal that site-selective deposition and epitaxial growth occurred during the photoreduction process.

To further investigate the detailed structure of the as-prepared matchlike ZnO/Au heterostructure, TEM measurements were performed as well. It can be clearly seen from Figure 2a that the tip of the ZnO nanorod is fully covered by spherical Au nanoparticles compared to the pristine ZnO nanorod (Figure S1 in the Supporting Information, SI). This is in agreement with the SEM observations. The HRTEM image and SAED pattern shown in Figure 2a−d confirm that the as-prepared ZnO nanorods are composed of single-crystalline structures and are defect-free. The measured fringe spacing is 0.242 nm, which corresponds to the (101) plane of the hexagonal phase ZnO.[30] The SAED pattern in the inset of Figure 2c also proves the single-crystalline nature of the as-prepared ZnO nanorod. Figure 2d presents the HRTEM image of the as-prepared matchlike ZnO/Au heterostructure. As can be seen, the surface-deposited Au nanoparticles have an average diameter of 6.5 ± 0.5 nm. Furthermore, the small-sized Au nanoparticles display a polycrystalline nature with different lattice orientations. The fringe spacing is ca. 0.201 nm, which corresponds to the (200) plane of a face-centered-cubic Au nanocrystal.[20] Noticeably, no other contaminations are

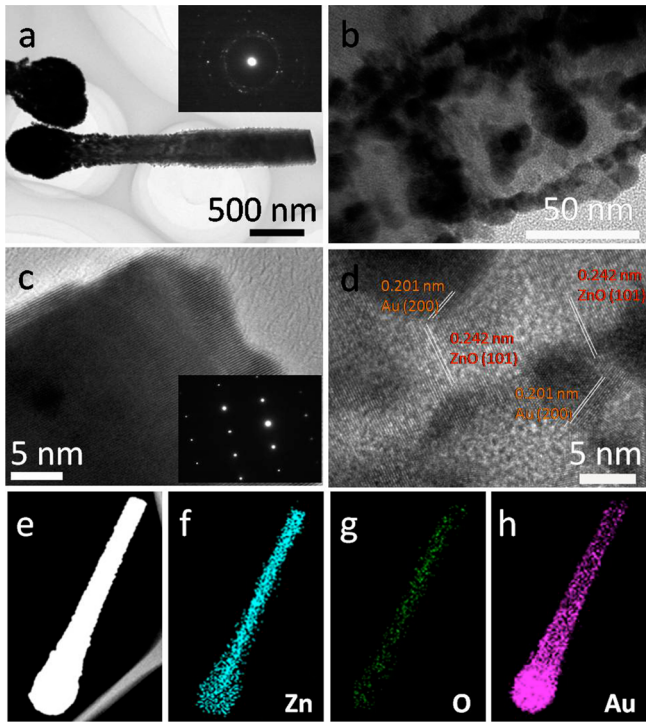

Figure 2. (a and b) TEM images of the typical matchlike ZnO/Au heterostructure. (c) HRTEM image of the ZnO nanorod. (d) HRTEM image of the typical matchlike ZnO/Au heterostructure. (e−h) STEM image and high-resolution element mappings of the ZnO/Au heterostructure. The insets of parts a and c present the SAED pattern of the typical ZnO/Au heterostructure and ZnO nanorod, respectively.

observed, possibly indicating that their interface between the ZnO nanorod and Au nanoparticles is "clean". Moreover, the SAED pattern shown as an inset in Figure 2a presents very bright concentric rings, which can be attributed to (111), (200), (220), and (311) planes from inner to outer, further suggesting that the decorated Au nanocrystals are polycrystalline. Parts e−h of Figure 2 show STEM-EDS element mapping of the heterostructure. As can be seen, the Zn (red) and O (green) elements are homogeneously distributed; however, the Au element (yellow) is mainly located in the tip region of the nanorods. The composition of the as-prepared matchlike heterostructure is further examined by energy-dispersive X-ray (EDX) measurement, as shown in Figure S2 in the SI. Besides the C and Cu signals arising from the copper grid, Zn, O, and Au peaks were identified, which is consistent with the heterostructure configuration. No other inorganic ligands, such as Cl, were found on the surface of the sample. Perhaps, the Cl was eliminated by sufficient washings, and the resultant Cl in the sample is lower than the detection limits of EDX measurement. The O/Zn and Au/Zn atomic ratios are about 1 and 0.032, as calculated from the EDX spectrum, respectively. The above results suggest that Au nanoparticles are decorated on the tip region of ZnO nanorods with a pure crystalline phase and are defect-free.

To investigate the morphological evolution of the matchlike ZnO/Au heterostructure, time-dependent experiments were carried out (Figure 3). At the initial photoreduction stage (0.5 h), a few of the Au nanoparticles are separately and randomly anchored on the tips of the ZnO nanorods, as shown in Figure 3a. With increasing reaction time to 1 h, Au nanoparticles are

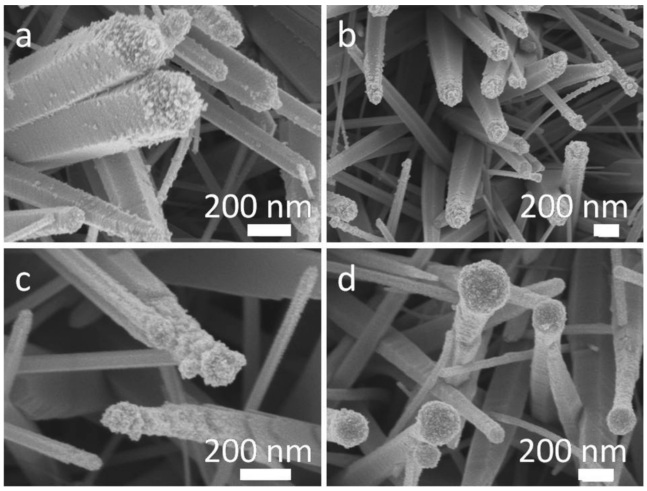

Figure 3. SEM images of the as-prepared ZnO/Au heterostructures obtained at different reaction stages of 30 min (a), 60 min (b), 120 min (c), and 180 min (d), respectively.

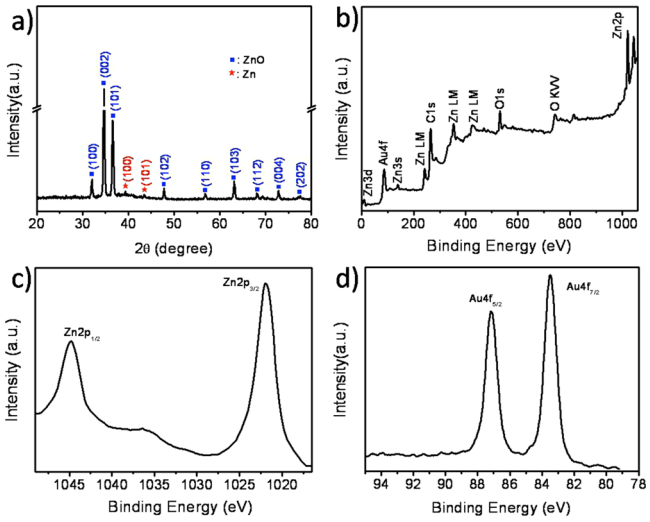

Figure 4. (a) XRD pattern. (b) Survey XPS spectrum of the typical matchlike ZnO/Au heterostructure. (c and d) High-resolution XPS spectra for Zn 2p and Au 4f, respectively.

fully covered on the tips of the ZnO nanorods (Figure 3b). After a reaction time of 2 h (Figure 3c), a Au bead is formed on the tips of the ZnO nanorods. With a further increase of the reaction time to 3 h, it can be observed from Figure 3d that the Au bead on the tip of the ZnO nanorod is not continuously increasing in size with prolonged reaction time but begins to deposit the small-sized Au nanoparticles. Therefore, it reveals that site-selective deposition of Au nanoparticles occurred during the photoreduction process. More specifically, the deposition sites of Au nanoparticles on ZnO nanorods can be tailored by adjusting the reaction time. The possible mechanism for the formation of a matchlike ZnO/Au heterostructure is explained as follows: the electrons are first generated in the conduction band of ZnO nanorods under illumination, as expressed in eq 1. The photoexcited electrons are known to be transported much faster along the *c* axis (the growth direction of ZnO nanorods) than other orientations (eq 2). As a result, the electrons are enriched at the tips of the ZnO nanorods, which can reduce the adsorbed Au^{3+} to Au^0, as shown in eq 3. Once the nucleation sites of Au nanocrystals are formed on the tips of the ZnO nanorods, the subsequent reduction of Au^{3+} would proceed at the preexisting nucleation sites and then result in the formation of a matchlike ZnO/Au heterostructure.

$$ZnO \rightarrow ZnO(e + h) \quad (1)$$

$$ZnO(e + h) \rightarrow e^- + h^+ \quad (2)$$

$$AuCl_4^- + 3e^- \rightarrow Au + 4Cl^- \quad (3)$$

The composition and crystalline structure of the as-prepared typical matchlike ZnO/Au heterostructure are further investigated by the XRD pattern and XPS measurement. Figure 4a exhibits the XRD pattern of the matchlike ZnO/Au heterostructure. It can be clearly seen that all diffraction peaks in the sample correspond to the standard diffraction of a hexagonal ZnO crystal (JCPDS 79-0206). Moreover, there are four weak peaks such as (100), (101), (102), and (103) planes in this pattern, which are attributed to the characteristic reflections of a Zn foil, confirming that ZnO nanorods are developed directly on the Zn foil substrate. The intense peaks at $2\theta = 34.52°$ for both samples are assigned to the (002) plane of the ZnO nanorods, further illustrating the vertical orientation of ZnO nanorod arrays. No impurity peaks are detected, further indicating the high purity of the product. However, the diffraction peaks in Figure 4a are similar to that of the pristine ZnO nanorod array shown in Figure S3 in the SI. No diffraction peaks of the Au nanocrystal are observed. It is probably due to the low content of the Au nanoparticles in the as-prepared heterostructure. In order to clarify the existence of metallic Au nanoparticles in the sample, XPS analysis is performed. The survey XPS spectrum in Figure 4b reveals the existence of Zn, O, Au, and C elements in the matchlike heterostructure. High-resolution spectra of Zn and Au species obtained from the matchlike sample are shown in parts c and d of Figure 4, respectively. The binding energy of Zn $2p_{3/2}$ at 1020.7 eV in Figure 4c is attributed to Zn^{2+},[31] which confirms that the Zn species exists mainly in the Zn^{2+} chemical state on the sample surface. The two peaks centered at 83.2 and 87.1 eV in Figure 4d can be attributed to Au $4f_{7/2}$ and Au $4f_{5/2}$, respectively. The peak position of Au $4f_{7/2}$ slightly shifts negative (0.8 eV) to lower binding energies compared with those of bulk Au ($4f_{7/2}$ at 84.0 eV). The binding energy shift of Au is mainly attributed to electron transfer from oxygen vacancies of ZnO to Au, leading to a lower binding energy of Au $4f_{7/2}$ in the matchlike ZnO/Au heterostructure.[32] Thus, the as-prepared matchlike ZnO/Au heterostructure with verified electron-transfer characteristics would create a high local electromagnetic response for improving the photoelectric activity.

The light-absorption ability of the as-prepared pristine ZnO nanorod array and the typical matchlike ZnO/Au heterostructure is shown in Figure 5a. As can be seen, the pristine ZnO nanorod array displayed a sharp absorption edge in the UV-light region with a wavelength below 390 nm due to their large band gap (3.4 eV). This coincides with the results previously reported by other groups.[33] However, after deposition of Au nanoparticles on ZnO nanorods, the absorption edge is extended to the visible-light region. Also, the absorption intensity is obviously strengthened, which is possibly due to the band-gap transition of the ZnO semiconductor.[34] The strong absorption band is centered at around 480 nm, probably corresponding to the localized SPR effect of the Au nanoparticles. The localized SPR peak is reported to be sensitive to the size, shape, and surrounding environment.[35] For

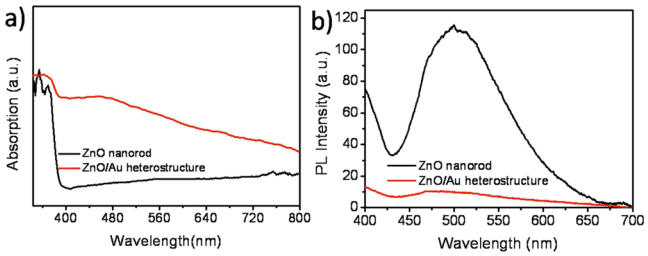

Figure 5. Diffuse reflectance UV−vis absorption spectra (a) and PL spectra (b) of the pristine ZnO nanorod and typical ZnO/Au heterostructure.

spherical Au nanoparticles with a size of 10 nm in an aqueous solution, their localized SPR peak is usually centered at 520 nm.[20,36] The localized SPR peak around 480 nm is probably due to the low refractive index of the ZnO nanorod (1.9).[37] This is another convincing proof that the Au nanoparticles modified on the ZnO nanorods and contributed to the visible-light absorption. Thus, because of the SPR effect of surface Au nanoparticles, such a unique matchlike heterostructure facilitates light harvesting. Figure 5b exhibits the room temperature PL spectra (excitation at 390 nm) of the as-prepared pristine ZnO nanorod array and matchlike ZnO/Au plasmonic heterostructure. The broad green emission around 540 nm can be assigned to the recombination of photoexcited holes, with electrons occupying the singly ionized oxygen vacancies in the ZnO nanorod surface.[38,39] After deposition of Au nanoparticles on the tips of the ZnO nanorods, the PL peak greatly decreased in intensity, which may be due to the electron trapping effect.[40] The plasmonic-enhanced heterostructure improves the separation of electrons and holes, indicating that their recombination has been suppressed. Therefore, the plasmonic effect is very beneficial to enhancing the photoactivity of the as-prepared matchlike ZnO/Au heterostructure.

PEC water splitting is used to evaluate the photoelectric performance of the as-prepared pristine ZnO nanorod array and matchlike ZnO/Au plasmonic heterostructure. Figure 6a shows the LSV curves of the as-prepared samples under full spectrum light illumination. As can be seen, the ZnO nanorod photoanode exhibits a very low dark current from 0 to 1.1 V (vs Ag/AgCl) in the range of 10^{-5} mA·cm^{-2}. Under illumination, the ZnO nanorod photoanode shows a pronounced photocurrent starting at 0.1 V and continues to increase to 0.33 mA·cm^{-2} at 1.0 V (vs Ag/AgCl). The matchlike ZnO/Au plasmonic heterostructure photoelectrode exhibits larger photocurrent density in the whole potential window than the corresponding pristine ZnO nanorod photoelectrode. The photocurrent density is as high as 9.11 mA·cm^{-2} at 1.0 V (vs Ag/AgCl). This result suggests that the deposition of Au nanoparticles on ZnO nanorods plays an important role in enhancing the photoelectrode activity. The photocurrent enhancement is explained as plasmonic-improved light absorption and quickened charge separation and transportation. Because of the SPR effect of the surface Au nanoparticles, the heterostructure absorbs the incident low-energy photons, which makes the absorption spectrum extend to the visible range with a significant enhancement of light harvesting. Meanwhile, the SPR-induced electromagnetic field effects facilitate electron and hole generation and separation.[41,42] When Au is replaced with Pt in the matchlike heterostructure, as shown in Figure S4 in the SI, the ZnO/Pt heterostructure also displays an enhancement of the PEC performance in the

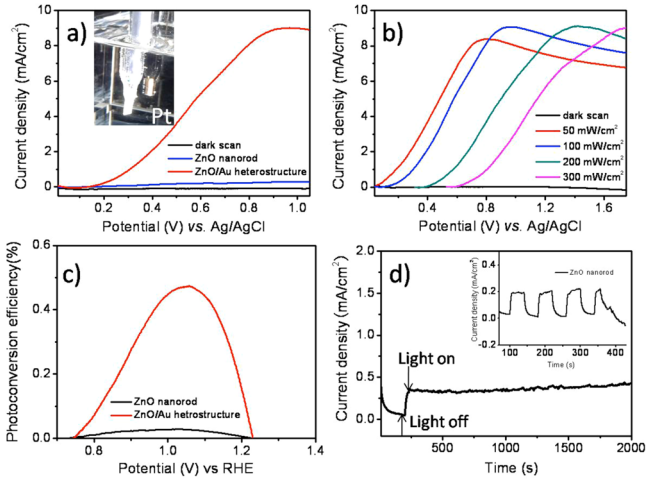

Figure 6. (a) LSV curves recorded for pristine ZnO nanorod arrays and the typical matchlike ZnO/Au heterostructure (the Au/Zn atomic ratio is 0.039) with a scan rate of 50 mV·s^{-1} in the applied potentials from 0 to +1.25 V under AM 1.5G simulated solar light at 100 mW·cm^{-2}. (b) LSV curves collected from the typical matchlike ZnO/Au heterostructure under different light power densities. (c) Photoconversion efficiency of the PEC cell with the ZnO nanorod and typical ZnO/Au heterostructure electrode as a function of the applied potential (vs RHE). (d) Photocurrent retention performance over 2000 s of the typical ZnO/Au heterostructure electrode at an applied voltage of +0.50 V vs Ag/AgCl under 100 mW·cm^{-2} light illumination. The inset exhibits the amperometric I−t curves of the pristine ZnO nanorod arrays with 50 s light on−off cycles.

potential range. However, the hydrogen generation ability of the ZnO/Pt heterostructure is smaller than that of the ZnO/Au heterostructure. Most importantly, Au nanoparticles with the plasmon effect coated on ZnO nanorods are more stable compared to Pt nanoparticles, which is very important for PEC measurements. In addition, power-dependence LSV curves, as shown in Figure 6b, show that the photocurrent density of the matchlike ZnO/Au heterostructure photoanode linearly increases with the incident light power. The result reveals a continuous photoelectric response of the photoelectrode with the light power density. This is very important for the development of practical solar-concentrated PEC cells.

Furthermore, the photoconversion efficiency (η) for PEC water splitting of the photoanode that requires an applied voltage can be evaluated using the following equation:[43]

$$\eta = \frac{I(1.23 - V_{app})}{P_{light}}$$

V_{app} is the applied external potential versus RHE. I is the externally measured current density at V_{app}. P_{light} is the power density of the incident light. The potential was measured against a Ag/AgCl reference and converted to RHE potential using the equation $E(\text{RHE}) = E(\text{Ag/AgCl}) + 0.1976V + 0.059\text{pH}$. As shown in Figure 6c, the maximum photoconversion efficiency of the pristine ZnO nanorod photoanode is 0.03% at an applied voltage of +1.03 V vs RHE, whereas the maximum efficiency of the matchlike ZnO/Au plasmonic heterostructure is as high as 0.48% at an applied voltage of +1.05 V vs RHE under the same conditions. The obtained value is slightly smaller than the result reported by Zhang et al., a high solar-to-hydrogen efficiency (0.52%) for plasmonic PEC water splitting. It is obtained from plasmonic Au nanoparticles

decorated on 3D-branched ZnO nanowire arrays.[44] Meanwhile, the efficiency is 16 times higher than that for the pristine ZnO nanorod. The enhanced PEC activities benefit from its unique feature of the matchlike ZnO/Au plasmonic heterostructure.

In addition to the generation of high photocurrent, the photostability of the electrodes is another key factor for the development of an efficient PEC hydrogen generation system. Thus, the stability of the photoanodes is also measured and exhibited in Figure 6d. It shows quick photocurrent decay for the pristine ZnO nanorod photoanode during 400 s. The reason for this low stability originates from the hole accumulation at the ZnO nanorods in operation, resulting in photocorrosion of the ZnO nanorods. The result can be confirmed from Figure S5 in the SI; the ZnO nanorods almost disappeared after PEC evaluation. However, the as-prepared ZnO/Au plasmonic heterostructure photoanode exhibits a very stable photoresponse with 2000 s of continuous light illumination. The matchlike ZnO/Au heterostructure is kept, and photocorrosion does not occur during the PEC measurement (Figure S5 in the SI). The reason for the stability difference is possibly that Au nanoparticles grafted on the tips of the ZnO nanorods can greatly separate the electrons and holes, protect the surface photocorrosion, and increase the stability. The results reveal that the high efficiency and good stability of a matchlike ZnO/Au plasmonic heterostructure can retain its original structure after long-term PEC water splitting.

To explain the energy conversion enhancement with the wavelength of incident light, incident photon-to-current efficiency (IPCE) measurements in the visible region for the pristine ZnO nanorod array and the matchlike ZnO/Au plasmonic heterostructure are performed (Figure 7). As reported, IPCE can be expressed as[45]

$$\mathrm{IPCE}\ (\%) = \frac{1240I}{\lambda P_{\mathrm{light}}} \times 100\%$$

where I is the photocurrent density ($\mathrm{mA\cdot cm^{-2}}$), λ is the incident light wavelength (nm), and P_{light} ($\mathrm{mW\cdot cm^{-2}}$) is the power density of monochromatic light at a specific wavelength. In comparison with the pristine ZnO nanorod array, the matchlike ZnO/Au plasmonic heterostructure shows an obviously enhanced IPCE performance and a red shift toward 500 nm, which is in accordance with its $J-V$ curves and the diffuse-reflectance characteristics. As can be seen, the IPCEs of the pristine ZnO nanorod array and matchlike ZnO/Au plasmonic heterostructure at an incident wavelength of 500 nm are 2.8 and 6.7%, respectively. The wavelength is closed to the prominent SPR absorption in the diffuse-reflectance UV–vis curve (Figure 5a). The IPCE is thought to be affected by the efficiencies of three fundamental processes including charge generation, charge transport within the material, and charge collection at the electrode/electrolyte interface.[45,46] Thus, the observed enhanced IPCE performance could be ascribed to the plasmonic-improved light absorption and resulted in a large increase in charge generation. Possibly, the good conductivity of Au nanoparticles also has an important role in enlarging the IPCE activity of the matchlike ZnO/Au heterostructure. The Au coating layer with an overall reduced charge-transfer resistance facilitates electron transfer from the ZnO nanorods to the electrolyte.

To confirm the contribution of the Au content on the photocurrent enhancement, PEC performances of the matchlike ZnO/Au plasmonic heterostructures with various Au/Zn ratios are carried out. Figure S6 in the SI shows the LSV curves of the as-prepared matchlike ZnO/Au plasmonic heterostructures with various Au/Zn ratios. The changes of the photocurrent densities measured at 1.0 V (vs Ag/AgCl) against the Au/Zn ratio are shown in Figure 8. The photocurrent densities of these photoanodes are enhanced as the Au/Zn ratio is increased from 0 to 0.023 and then decreased with further increases of the ratio. When the ratio of Au/Zn in the heterostructure is 0.023, the photocurrent density achieves the maximum (10.90 $\mathrm{mA\cdot cm^{-2}}$). The improved photocurrent with an increased Au/Zn ratio is believed to be the result of extending the light absorption range and improving the separation of electrons and holes. However, excessive deposition would possibly make Au nanoparticles the center for electron and hole fast recombination, resulting in photocurrent decay.

To discover the relationship between a matchlike ZnO/Au plasmonic heterostructure and the enhanced photocurrent and IPCE performances, electrochemical impedance measurements are carried out. The capacitance is obtained at each potential with 10 kHz frequency in the dark. Mott–Schottky plots are generated from the capacitance values. Both of the samples show a positive slope in the Mott–Schottky plots, indicating that they are n-type semiconductors with electrons as majority carriers (Figure 9a). The slopes determined from the Mott–

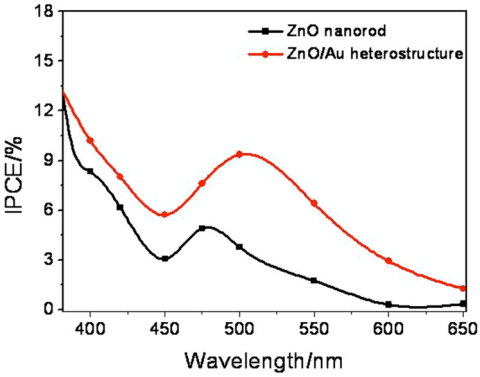

Figure 7. IPCE curves for the pristine ZnO nanorod array and matchlike ZnO/Au plasmonic heterostructure photoanode measured in the wavelength range from 380 to 600 nm at an applied voltage of +0.60 V vs Ag/AgCl.

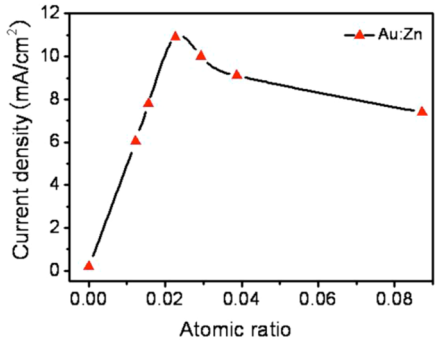

Figure 8. Plot of the obtained photocurrent density as a function of the ZnO/Au heterostructure photoanode with various Au/Zn atomic ratios at a scan rate of 50 $\mathrm{mV\cdot s^{-1}}$ under 100 $\mathrm{mW\cdot cm^{-2}}$ light illumination.

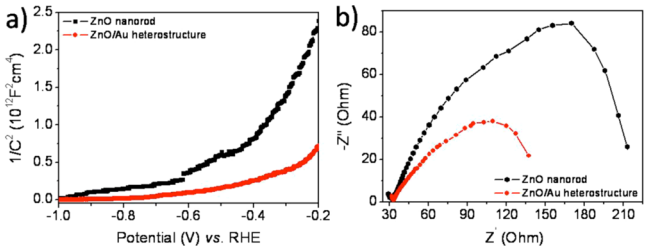

Figure 9. (a) Mott–Schottky plots of the pristine ZnO nanorod array and typical ZnO/Au heterostructure in the dark at a frequency of 1 kHz and an ac current of 5 mV with a three-electrode system. (b) Nyquist plots of electrochemical impedance spectra of the pristine ZnO nanorod array and typical ZnO/Au heterostructure photoanode measured at 10 mV (vs Ag/AgCl) in a 0.1 M Na_2SO_4 aqueous solution in the dark.

Schottky plots are used to estimate the carrier density using the following equation:

$$N_d = (2/e_0\varepsilon\varepsilon_0)[d(1/C^2)/dV]^{-1}$$

where e_0 is the electron charge, ε the dielectric constant of ZnO, ε_0 the permittivity of the vacuum, N_d the dopant density, and V the potential applied at the electrode. With an ε value of 10 for ZnO and the permittivity of the vacuum (ε_0 = 8.85 × 10^{-14} F·cm^{-1}), the electron densities of the pristine ZnO nanorod array and matchlike ZnO/Au plasmonic heterostructure photoanodes are estimated to be 1.88 × 10^{18} and 1.78 × 10^{19} cm^{-3}, respectively. The ZnO/Au plasmonic heterostructure exhibits an increase of about 9.5 orders of magnitude in the carrier density compared to the pristine ZnO nanorod array. The enlarged electron density in the ZnO/Au plasmonic heterostructure is believed to be a major contributing factor for the pronounced photocurrent density enhancement.

Moreover, electrochemical impedance spectroscopy was employed to investigate the oxidation process kinetics at the electrode surface. Nyquist plots collected for the photoanodes exhibit a capacitive arc in the dark, suggesting that the Faradaic charge transfer is limiting for the oxidation process at the electrode surface (Figure 9b). Obviously, the arc diameter for the typical ZnO/Au heterostructure is much smaller than that of the pristine ZnO nanorod array. This indicates that Au nanoparticles enhance the electron mobility by suppressing the recombination of photoexcited electrons and holes in the ZnO/Au heterostructure photoanode. The reduced charge-transfer resistance is thought to be another key factor for enhancing the PEC performance of the matchlike ZnO/Au heterostructure.

On the basis of the above results, the electron-transfer mechanism of the matchlike ZnO/Au plasmonic heterostructure in PEC water splitting has been proposed, as shown in Scheme 1. As convinced by the XRD pattern and HRTEM image, the pristine ZnO nanorods show single-crystalline structure and a clean interface with Au nanoparticles. It is reported that the defect-free well-crystallized structure can help to improve the charge-transfer efficiency.[47] Meanwhile, the well-defined interface between ZnO nanorods and Au nanoparticles can also play important roles in their photoactivity enhancement. When Au nanoparticles are anchored on the tips of the ZnO nanorods, the electrons are photoexcited from the valence band to the conduction band of the ZnO nanorods, with the same amount of holes left behind in the valence band. Then because the newly formed Fermi energy level of the heterostructures is lower than the energy level of the bottom of the conduction band of the ZnO nanorod, the photoexcited electrons would be transferred from ZnO to Au driven by the energy difference to reduce their recombination. A theoretical calculation reported by Han et al. confirmed the presence of abundant empty states within the ZnO band gap in ZnO/Au composites.[48] Meanwhile, because of SPR excitation, Au nanoparticles absorb the resonant photons to generate hot electrons. At last, the leaving holes in the valence band of the ZnO nanorods are immediately consumed to produce oxygen, and the electrons are injected into the Pt electrode via the conduction band of ZnO nanorods to generate hydrogen.

Scheme 1. (a) Schematics of the PEC Cell[a] and (b) Schematic Illustration of the Enhanced Light-Harvesting and Charge-Separation Process of the Typical ZnO/Au Plasmonic Heterostructure Photoanode

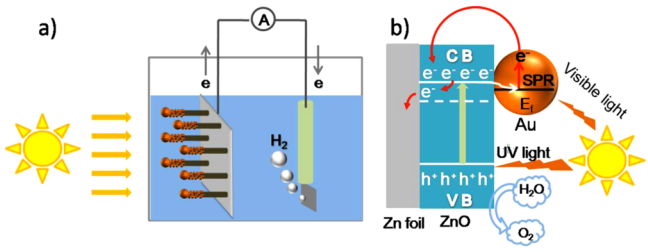

[a]The as-prepared nanostructure serves as the anode, saturated Ag/AgCl as the reference electrode, and Pt foil as the counter electrode for hydrogen evolution.

4. CONCLUSIONS

In summary, the matchlike ZnO/Au plasmonic heterostructure as the photoanode for PEC water splitting has been prepared via a facile and large-scale two-step method. The content and deposition site of Au nanoparticles can be controlled by varying the precursor concentration and reaction time. In comparison to the pristine ZnO nanorod array, the matchlike ZnO/Au heterostructure photoanode shows a plasmonic-enhanced photocurrent density and IPCE performance. The heterostructure presents the highest photocurrent density of 9.11 mA·cm^{-2} at a low bias of 1.0 V (vs Ag/AgCl) and the highest efficiency of 0.48%, which is 16 times higher than that of the pristine ZnO nanorod array. Also, the IPCE reaches 6.7% at 500 nm, over 2 times higher than that of the pristine ZnO nanorod array. These results provide useful insight into the design of unique plasmonic semiconductor/metal heterostructure photoanodes for solar harvesting.

■ ASSOCIATED CONTENT

Ⓢ Supporting Information

Supplementary figures (Figures S1–S6). This material is available free of charge via the Internet at http://pubs.acs.org.

■ AUTHOR INFORMATION

Corresponding Authors

*E-mail: lichuanhao1983@163.com.
*E-mail: lishikuo@ahu.edu.cn.

Notes

The authors declare no competing financial interest.

■ ACKNOWLEDGMENTS

This work is supported by the National Science Foundation of China (Grants 51202001, 21301001, and 21303002), the Key Project of Anhui Provincial Education Department (Project KJ2011A021), Anhui Provincial Natural Science Foundation (Grants 1208085QB43, 1208085QB35, and 11040606Q01), the Research Fund for the Doctoral Program of Higher Education of China (Grant 20123401120004), and the Youth Backbone Program of Anhui University.

■ REFERENCES

(1) Mor, G. K.; Shankar, K.; Paulose, M.; Varghese, O. K.; Grimes, C. A. Enhanced Photocleavage of Water Using Titania Nanotube Arrays. *Nano Lett.* **2005**, *5*, 191−195.

(2) Youngblood, W. J.; Lee, S.-H. A.; Kobayashi, Y.; Hernandez-Pagan, E. A.; Hoertz, P. G.; Moore, T. A.; Moore, A. L.; Gust, D.; Mallouk, T. E. Photoassisted Overall Water Splitting in a Visible Light-Absorbing Dye-Sensitized Photoelectrochemical Cell. *J. Am. Chem. Soc.* **2009**, *131*, 926−927.

(3) Wang, G.; Ling, Y.; Wang, H.; Yang, X.; Wang, C.; Zhang, J. Z.; Li, Y. Hydrogen-Treated WO_3 Nanoflakes Show Enhanced Photostability. *Energy Environ. Sci.* **2012**, *5*, 6180−6187.

(4) Zhang, P.; Kleiman-Shwarsctein, A.; Hu, Y.-S.; Lefton, J.; Sharma, S.; Forman, A. J.; McFarland, E. Oriented Ti Doped Hematite Thin Film as Active Photoanodes Synthesized by Facile APCVD. *Energy Environ. Sci.* **2011**, *4*, 1020−1028.

(5) Cho, I. S.; Chen, Z.; Forman, A. J.; Kim, D. R.; Rao, P. M.; Jaramillo, T. F.; Zheng, X. Branched TiO_2 Nanorods for Photoelectrochemical Hydrogen Production. *Nano Lett.* **2011**, *11*, 4978−4984.

(6) Wang, G.; Ling, Y.; Wheeler, D. A.; George, K. E.; Horsley, K.; Heske, C.; Zhang, J. Z.; Li, Y. Facile Synthesis of Highly Photoactive α-Fe_2O_3-based Films for Water Oxidation. *Nano Lett.* **2011**, *11*, 3503−3509.

(7) Qiu, Y.; Yan, K.; Deng, H.; Yang, S. Secondary Branching and Nitrogen Doping of ZnO Nanotetrapods: Building a Highly Active Network for Photoelectrochemical Water Splitting. *Nano Lett.* **2011**, *12*, 407−413.

(8) Qin, D.-D.; Tao, C.-L.; Friesen, S. A.; Wang, T.-H.; Varghese, O. K.; Bao, N.-Z.; Yang, Z.-Y.; Mallouk, T. E.; Grimes, C. A. Dense Layers of Vertically Oriented WO_3 Crystals as Anodes for Photoelectrochemical Water Oxidation. *Chem. Commun.* **2012**, *48*, 729−731.

(9) Su, J.; Feng, X.; Sloppy, J. D.; Guo, L.; Grimes, C. A. Vertically Aligned WO_3 Nanowire Arrays Grown Directly on Transparent Conducting Oxide Coated Glass: Synthesis and Photoelectrochemical Properties. *Nano Lett.* **2010**, *11*, 203−208.

(10) Sun, K.; Jing, Y.; Li, C.; Zhang, X.; Aguinaldo, R.; Kargar, A.; Madsen, K.; Banu, K.; Zhou, Y.; Bando, Y. 3D Branched Nanowire Heterojunction Photoelectrodes for High-efficiency Solar Water Splitting and H_2 Generation. *Nanoscale* **2012**, *4*, 1515−1521.

(11) Wolcott, A.; Smith, W. A.; Kuykendall, T. R.; Zhao, Y.; Zhang, J. Z. Photoelectrochemical Study of Nanostructured ZnO Thin Films for Hydrogen Generation From Water Splitting. *Adv. Funct. Mater.* **2009**, *19*, 1849−1856.

(12) Kim, H.; Seol, M.; Lee, J.; Yong, K. Highly Efficient Photoelectrochemical Hydrogen Generation Using Hierarchical ZnO/WO_X Nanowires Cosensitized with CdSe/CdS. *J. Phys. Chem. C* **2011**, *115*, 25429−25436.

(13) Yang, X.; Wolcott, A.; Wang, G.; Sobo, A.; Fitzmorris, R. C.; Qian, F.; Zhang, J. Z.; Li, Y. Nitrogen-Doped ZnO Nanowire Arrays for Photoelectrochemical Water Splitting. *Nano Lett.* **2009**, *9*, 2331−2336.

(14) Kaidashev, E.; Lorenz, M.; Von Wenckstern, H.; Rahm, A.; Semmelhack, H.-C.; Han, K.-H.; Benndorf, G.; Bundesmann, C.; Hochmuth, H.; Grundmann, M. High Electron Mobility of Epitaxial ZnO Thin Films on *c*-plane Sapphire Grown by Multistep Pulsed-Laser Deposition. *Appl. Phys. Lett.* **2003**, *82*, 3901−3903.

(15) Liu, C.; Dasgupta, N. P.; Yang, P. Semiconductor Nanowires for Artificial Photosynthesis. *Chem. Mater.* **2014**, *26*, 415−422.

(16) Feng, X.; Shankar, K.; Varghese, O. K.; Paulose, M.; Latempa, T. J.; Grimes, C. A. Vertically Aligned Single Crystal TiO_2 Nanowire Arrays Grown Directly on Transparent Conducting Oxide Coated Glass: Synthesis Details and Applications. *Nano Lett.* **2008**, *8*, 3781−3786.

(17) Shankar, K.; Basham, J. I.; Allam, N. K.; Varghese, O. K.; Mor, G. K.; Feng, X.; Paulose, M.; Seabold, J. A.; Choi, K.-S.; Grimes, C. A. Recent Advances in the Use of TiO_2 Nanotube and Nanowire Arrays for Oxidative Photoelectrochemistry. *J. Phys. Chem. C* **2009**, *113*, 6327−6359.

(18) Linic, S.; Christopher, P.; Ingram, D. B. Plasmonic-Metal Nanostructures for Efficient Conversion of Solar to Chemical Energy. *Nat. Mater.* **2011**, *10*, 911−921.

(19) Dou, D.; Park, J. G.; Rana, S.; Madden, B. J.; Jiang, H.; Pang, Y.-P. Novel Selective and Irreversible Mosquito Acetylcholinesterase Inhibitors for Controlling Malaria and Other Mosquito-Borne Diseases. *Sci. Rep.* **2013**, *3*, 1−11.

(20) Pu, Y.-C.; Wang, G.; Chang, K.-D.; Ling, Y.; Lin, Y.-K.; Fitzmorris, B. C.; Liu, C.-M.; Lu, X.; Tong, Y.; Zhang, J. Z. Au Nanostructure-Decorated TiO_2 Nanowires Exhibiting Photoactivity Across Entire UV−visible Region for Photoelectrochemical Water Splitting. *Nano Lett.* **2013**, *13*, 3817−3823.

(21) Warren, S. C.; Thimsen, E. Plasmonic Solar Water Splitting. *Energy Environ. Sci.* **2012**, *5*, 5133−5146.

(22) Hou, W.; Cronin, S. B. A Review of Surface Plasmon Resonance-Enhanced Photocatalysis. *Adv. Funct. Mater.* **2013**, *23*, 1612−1619.

(23) Bi, Y.; Lu, G.; Ye, J.; Wang, T.; Jiao, Z.; Chen, T.; Lin, S.; Li, Y.; Ren, W. Vertically Aligned ZnO Nanowire Arrays Tip-Grafted with Silver Nanoparticles for Photoelectrochemical Applications. *Nanoscale* **2013**, *5*, 7552−7557.

(24) Su, F.; Wang, T.; Lv, R.; Zhang, J.; Zhang, P.; Lu, J.; Gong, J. Dendritic Au/TiO_2 Nanorod Arrays for Visible-Light Driven Photoelectrochemical Water Splitting. *Nanoscale* **2013**, *5*, 9001−9009.

(25) Zhou, X.; Liu, G.; Yu, J.; Fan, W. Surface Plasmon Resonance-Mediated Photocatalysis by Noble Metal-Based Composites under Visible Light. *J. Mater. Chem.* **2012**, *22*, 21337−21354.

(26) Lan, J.; Zhou, X.; Liu, G.; Yu, J.; Zhang, J.; Zhi, L.; Nie, G. Enhancing Photocatalytic Activity of One-Dimensional $KNbO_3$ Nanowires by Au Nanoparticles under Ultraviolet and Visible-light. *Nanoscale* **2011**, *3*, 5161−5167.

(27) Wang, X.; Peng, K.-Q.; Hu, Y.; Zhang, F.-Q.; Hu, B.; Li, L.; Wang, M.; Meng, X.; Lee, S.-T. Silicon/Hematite Core/shell Nanowire Array Decorated with Gold Nanoparticles for Unbiased Solar Water Oxidation. *Nano Lett.* **2014**, *14*, 18−23.

(28) Zhang, Z.; Zhang, L.; Hedhili, M. N.; Zhang, H.; Wang, P. Plasmonic Gold Nanocrystals Coupled with Photonic Crystal Seamlessly on TiO_2 Nanotube Photoelectrodes for Efficient Visible Light Photoelectrochemical Water Splitting. *Nano Lett.* **2012**, *13*, 14−20.

(29) Wu, Z.; Xu, C.; Wu, Y.; Yu, H.; Tao, Y.; Wan, H.; Gao, F. ZnO Nanorods/Ag Nanoparticles Heterostructures with Tunable Ag Contents: a Facile Solution-Phase Synthesis and Applications in Photocatalysis. *CrystEngComm* **2013**, *15*, 5994−6002.

(30) Gupta, M. K.; Lee, J.-H.; Lee, K. Y.; Kim, S.-W. Two-Dimensional Vanadium-Doped ZnO Nanosheet-Based Flexible Direct Current Nanogenerator. *ACS Nano* **2013**, *7*, 8932−8939.

(31) Vamathevan, V.; Amal, R.; Beydoun, D.; Low, G.; McEvoy, S. Photocatalytic Oxidation of Organics in Water Using Pure and Silver-Modified Titanium Dioxide Particles. *J. Photochem. Photobiol., A* **2002**, *148*, 233−245.

(32) Wu, Y.; Liu, H.; Zhang, J.; Chen, F. Enhanced Photocatalytic Activity of Nitrogen-Doped Titania by Deposited with Gold. *J. Phys. Chem. C* **2009**, *113*, 14689−14695.

(33) Lu, X.; Wang, G.; Xie, S.; Shi, J.; Li, W.; Tong, Y.; Li, Y. Efficient Photocatalytic Hydrogen Evolution Over Hydrogenated ZnO Nanorod Arrays. *Chem. Commun.* **2012**, *48*, 7717−7719.

(34) Primo, A.; Marino, T.; Corma, A.; Molinari, R.; Garcia, H. Efficient Visible-Light Photocatalytic Water Splitting by Minute Amounts of Gold Supported on Nanoparticulate CeO_2 Obtained by a Biopolymer Templating Method. *J. Am. Chem. Soc.* **2011**, *133*, 6930−6933.
(35) Li, J.; Cushing, S. K.; Bright, J.; Meng, F.; Senty, T. R.; Zheng, P.; Bristow, A. D.; Wu, N. Ag@Cu_2O Core−Shell Nanoparticles as Visible-Light Plasmonic Photocatalysts. *ACS Catal.* **2012**, *3*, 47−51.
(36) Liu, L.; Ouyang, S.; Ye, J. Gold-Nanorod-Photosensitized Titanium Dioxide with Wide-Range Visible-Light Harvesting Based on Localized Surface Plasmon Resonance. *Angew. Chem., Int. Ed.* **2013**, *125*, 6821−6825.
(37) Li, J.; Cushing, S. K.; Zheng, P.; Senty, T.; Meng, F.; Bristow, A. D.; Manivannan, A.; Wu, N. Solar Hydrogen Generation by a CdS−Au−TiO_2 Sandwich Nanorod Array Enhanced with Au Nanoparticle as Electron Relay and Plasmonic Photosensitizer. *J. Am. Chem. Soc.* **2014**, *136*, 8438−8449.
(38) Wang, H.; Bai, Y.; Zhang, H.; Zhang, Z.; Li, J.; Guo, L. CdS Quantum Dots-Sensitized TiO_2 Nanorod Array on Transparent Conductive Glass Photoelectrodes. *J. Phys. Chem. C* **2010**, *114*, 16451−16455.
(39) Ye, M.; Gong, J.; Lai, Y.; Lin, C.; Lin, Z. High-Efficiency Photoelectrocatalytic Hydrogen Generation Enabled by Palladium Quantum Dots-Sensitized TiO_2 Nanotube Arrays. *J. Am. Chem. Soc.* **2012**, *134*, 15720−15723.
(40) Georgekutty, R.; Seery, M. K.; Pillai, S. C. A Highly Efficient Ag-ZnO Photocatalyst: Synthesis, Properties, and Mechanism. *J. Phys. Chem. C* **2008**, *112*, 13563−13570.
(41) Liu, Z.; Hou, W.; Pavaskar, P.; Aykol, M.; Cronin, S. B. Plasmon Resonant Enhancement of Photocatalytic Water Splitting under Visible Illumination. *Nano Lett.* **2011**, *11*, 1111−1116.
(42) Li, H.; Lu, W.; Tian, J.; Luo, Y.; Asiri, A. M.; Al-Youbi, A. O.; Sun, X. Synthesis and Study of Plasmon-Induced Carrier Behavior at Ag/TiO_2 Nanowires. *Chem.—Eur. J.* **2012**, *18*, 8508−8514.
(43) Walter, M. G.; Warren, E. L.; McKone, J. R.; Boettcher, S. W.; Mi, Q.; Santori, E. A.; Lewis, N. S. Solar Water Splitting Cells. *Chem. Rev.* **2010**, *110*, 6446−6473.
(44) Zhang, X.; Liu, Y.; Kang, Z. 3D Branched ZnO Nanowire Arrays Decorated with Plasmonic Au Nanoparticles for High-Performance Photoelectrochemical Water Splitting. *ACS Appl. Mater. Interfaces* **2014**, *6*, 4480−4489.
(45) Chen, Z.; Jaramillo, T. F.; Deutsch, T. G.; Kleiman-Shwarsctein, A.; Forman, A. J.; Gaillard, N.; Garland, R.; Takanabe, K.; Heske, C.; Sunkara, M. Accelerating Materials Development for Photoelectrochemical Hydrogen Production: Standards for Methods, Definitions, and Reporting Protocols. *J. Mater. Res.* **2010**, *25*, 3−16.
(46) Pan, K.; Dong, Y.; Zhou, W.; Pan, Q.; Xie, Y.; Xie, T.; Tian, G.; Wang, G. Facile Fabrication of Hierarchical TiO_2 Nanobelt/ZnO Nanorod Heterogeneous Nanostructure: An Efficient Photoanode for Water Splitting. *ACS Appl. Mater. Interfaces* **2013**, *5*, 8314−8320.
(47) Chen, Y.; Zeng, D.; Zhang, K.; Lu, A.; Wang, L.; Peng, D.-L. Au−ZnO Hybrid Nanoflowers, Nanomultipods and Nanopyramids: One-Pot Reaction Synthesis and Photocatalytic Properties. *Nanoscale* **2014**, *6*, 874−881.
(48) Yao, K. X.; Liu, X.; Zhao, L.; Zeng, H. C.; Han, Y. Site-Specific Growth of Au Particles on ZnO Nanopyramids under Ultraviolet Illumination. *Nanoscale* **2011**, *3*, 4195−4200.